PROCEEDINGS OF SCIENCE

Status, Calibration, and Cosmic Ray Detection of ARIANNA-HCR Station

Shih-Hao Wang* **for the TAROGE and the ARIANNA Collaborations**†
Graduate Institute of Physics and Leung Center for Cosmology and Particle Astrophysics, National Taiwan University, No. 1, Sec. 4, Roosevelt Rd., Taipei 10617, Taiwan, R.O.C.

E-mail: wsh4180@gmail.com

The ARIANNA Horizontal Cosmic Ray (HCR) station is an antenna array in Antarctica for detecting radio impulses emitted from inclined extensive air showers (EAS) above about 300 PeV generated by cosmic rays and ultra-high energy Earth-skimming tau neutrinos coming out from nearby mountains. The station has 8 log-periodic dipole antennas above the ice, pointing horizontally toward the mountain ridges, with bandwidth of 110-500 MHz and improved performance after upgrade from its prototype in November 2017, and has been continuously operating over almost the entire austral summer. The timing and angular resolution, which are crucial for discriminating between cosmic ray and neutrino events, are calibrated with ground-based transmitters both nearby the station and on the mountain. We will discuss the interference from reflected signal from the ice, which becomes apparent for signals from lower elevation angles ($< 25^\circ$), complicating the event reconstruction but also providing additional angular information. We will summarize its instrumentation and operation in the 2017-2018 season, and report the result of the search of cosmic-ray EAS candidates and their angular distribution.

36th International Cosmic Ray Conference -ICRC2019-
July 24th - August 1st, 2019
Madison, WI, U.S.A.

*Speaker.
†for collaboration list see PoS(ICRC2019)1177

PoS(ICRC2019)462

1. Introduction

Radio detection of extensive air showers (EAS) initiated by high energy cosmic rays of energy above 10^{16} eV has been established and cross-calibrated with other conventional detection methods and simulation, and is capable of extracting cosmic-ray parameters such as direction, energy and composition (see [1] for a review). The main mechanism of such radio emission is the deflection of electrons and positrons in air shower under the geomagnetic field, producing coherent pulse with duration of order of 10 ns and linearly polarized along the direction of Lorentz force, relativistically beamed in the forward direction with opening angle typically about 1°. While the majority of the EAS radio observatories operate at lower frequencies 30–80 MHz for the benefit of coherent emission, standalone radio observatories looking for ultra-high energy (UHE) neutrino signal in Antarctic ice such as ANITA [2] and ARIANNA [3, 4], utilising higher frequency band at 100–1000 MHz, have also detected cosmic-ray EAS signals. In addition, ultra-high energy (UHE) Earth-skimming tau neutrino (ν_τ) can also generate EAS if having charged-current interaction within rock followed by tau lepton decay in the air. Recently, two intriguing up-going ν_τ -like events observed by ANITA [5] call for further confirmation by other experiments.

Besides the radio-quietness and strong, nearly vertical geomagnetic field in Antarctica, the vast Transantarctic Mountains can serve as extra target volume for neutrino interaction, if an antenna array pointing toward the mountains is built at a proper distance for the tau lepton to decay and the air shower to develop [6]. This makes Antarctica an ideal place for detecting inclined air showers from both cosmic rays and neutrinos.

The ARIANNA horizontal cosmic ray (HCR) station is designed for investigating the potential of such a detector. Located at Ross Ice Shelf in Antarctica together with in-ice ARIANNA hexagonal radio array (HRA) stations [8, 9], the station is an above-ice antenna array pointing horizontally toward Mt. Discovery (Fig. 1). Its prototype had been deployed in 2016 and previously reported [7], and was upgraded to full-scale station in November, 2017, and has been operating smoothly in 2017–18 and 2018–19 season. In this paper we report the development since then, and the progress on the simulation and the search for inclined cosmic rays.

2. Station Setup

The HCR station is based on the ARIANNA hardware (see [3, 9] for details) but equipped with eight log-periodic dipole array (LPDA) antennas of bandwidth at 110–600 MHz and 7 dBi gain installed above the snow, in the configuration as shown in Fig. 1. Six of the antennas are horizontally polarized (Hpol) to be aligned with the polarization of geomagnetic emission, while the other two are vertically polarized (Vpol) for the polarization measurement.

The received signals are passed through 100–500 MHz band-pass filters and amplifiers of 55 dB gain, and processed by the data-acquisition (DAQ) system right below the snow. The core parts of DAQ circuit board are two Synchronous Sampling plus Triggering chips [10] providing 8-channel inputs. The SST board can store 256 samples for each channel with 12-bits dynamic range, possessing timing precision between samples and channels of picosecond level, and its sampling rate set at 1 GHz for EAS detection. The trigger at channel level is formed when its signal passes both positive and negative thresholds within 5 ns, where the thresholds are set at roughly ± 4 times

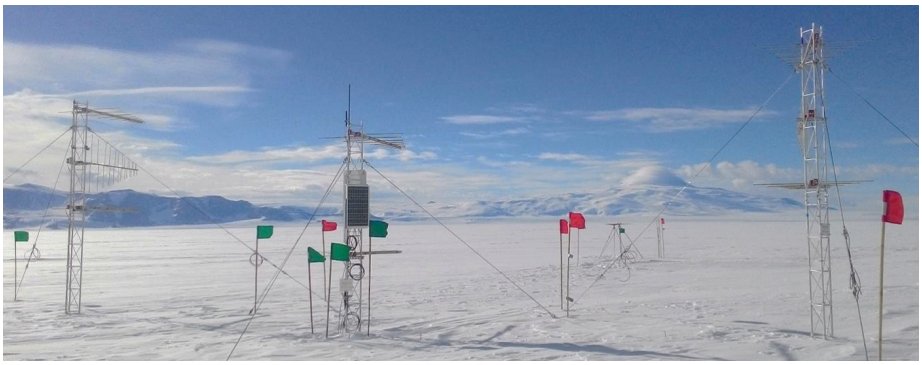

Figure 1: The ARIANNA-HCR station. The eight LPDA antennas are mounted on three towers of 7m apart. The left and right towers have antennas 2.2 m above the surface and 1m spacing with (H, V, H) configuration. The middle tower with 2 Hpol was installed with the prototype in 2016, and is lower due to snow accumulation. A transmitter antenna is placed 26 m away in front of the station for calibration. The station points to Mt. Discovery (2,681 m) 40 km away in the background, on which the other calibration pulser is installed.

of RMS noise voltage. Then the station level trigger requires 3-out-of-8 coincidence of channel triggers within 32 ns for the waveforms to be digitized and recorded. An additional level-1 (L1) trigger is applied on the microprocessor for vetoing narrow-band noises online, by computing the ratio of the peak magnitude of the FFT spectrum to the sum of the rest of spectrum. An event is rejected if the value exceeds a given threshold of 0.3 at any channel. With the above setting, the event rate typically ranges from 10^{-3} to 1 Hz within a day due to the variation of the galactic radio background. To monitor the RF background, a forced trigger at every 67 seconds is enabled to obtain unbiased noise samples.

The autonomous station is powered entirely by solar panels and $LiFePO_4$ batteries, with merely 4W power consumption. This ensures the station can operate throughout austral summer typically from mid September to mid April. Via long-range Wi-Fi and Iridium satellite communications, the station can be remotely configured and transfer data back to the server in the US in nearly real time.

3. Event Reconstruction and Calibration with Pulsers

The source direction of an event is reconstructed with the time difference of arrival (TDOA) of signals between Hpol channels, based on an interferometric method similar to that in [11]. The TDOA of each antenna pair is extracted by cross-correlating the waveforms. In this analysis, waveforms are first interpolated by a factor of 20, and then cross-correlated within a time window around the peak of each one to reduce the bias from noise. The time window is either 100 ns long for original waveforms or 10 ns long if the direction is known (e.g. for pulser events) and both the antenna and the amplifier responses can be deconvolved. The reconstructed angles are in the direction for which the TDOAs of all pairs give the highest sum of correlation coefficients.

The timing offset and resolution of each antenna pair are calibrated with a transmitter antenna (pulser) placed at six different locations about 26 m away, scanning several angles from the station. Since the pulser is fixed at known positions, the timing resolution of about 40 ps is obtained from

the spread of TDOA distribution of pulser events. The internal fixed time delay of each channel, is calibrated with the angle scan. The residual timing offset of each channel is controlled within 0.2 ns, which is likely due to positioning error of antennas.

After the deconvolution, the pulse waveform is found to have a weaker and delayed pulse consistent with reflection from the snow surface. Simulation suggests that the interference from reflected signal is not negligible for zenith angle larger than 65°, due to increasing reflection coefficient > 0.3 and delay of order of nanoseconds. The delay of upper and lower channels are different , causing the interfered waveforms losing similarity, and thus bias the correlation and resulting TDOA and reconstruction. The effect was also found in prototype with HiCal-2 ballone-borne pulser [7]. This is the other reason a narrower time window is applied for deconvolved case for obtaining better timing measurement.

The other pulser system was installed on Mt. Discovery at altitude of 1,993 m, with 40 km distance and 2.7° elevation angle from the station, for studying the propagation in nearly horizontal directions, calibrating the azimuthal orientation of the station and verifying event reconstruction. The design of the pulser instrument inherits from that of HiCal-2 [12], by which the HCR prototype was calibrated, but equipped with two sets of bicone antennas, one at Hpol and one at Vpol. The pulser was running on a small solar panel and batteries during 2018-01-16 to 2018-01-26, pulsing at a rate of about 0.3 Hz, and the pulses were successfully received by the station (see Fig. 4). The pulse events are identified with time stamp, high correlation value and fixed TDOA. After reconstructing these pulses an angular resolution of $\sigma_\theta = 0.33°$ in zenith and $\sigma_\phi = 0.03°$ in azimuth is derived, showing improvement from the prototype station: $(\sigma_\theta, \sigma_\phi) = (0.63°, 1.42°)$. The reasons are increased number of channels (3 to 6 Hpols) for reconstruction and the horizontal baseline (max 3 m to 14 m). There is a systematic offset at reconstructed zenith of $-0.5°$, which is likely due to reflection interference and is under investigation.

4. Simulation and Expected Event Distribution

To get the expected event rate and angular distribution for cosmic rays, a Monte-Carlo simulation is constructed following similar procedures described in [3]. Radio emission of air shower is simulated with CoREAS [13]. A set of 2,041 proton-initiated showers are generated with energy scanned over $\log_{10}(E\ [\text{eV}]) = 16.5$–$19.5$, and angles over all forward-coming directions ($\theta = [0°, 90°]$, $\phi = [0°, 180°]$), with radiated electric field on the ground plane sampled with a star-shaped array. The station position relative to the shower axis is randomly selected within the simulated area, and the incident electric field to each channel is assumed to be the same because of relatively small antenna spacing. The reflected signal is added depending on the incoming direction and height of the antenna, assuming a flat snow surface with refractive index of 1.3, following Fresnel's equations. For the receiver response, HFSS software [14] is used to model the LPDA antenna in free space. Since the back lobes of the antenna are hard to model due to the presence of tower, only air showers coming from the front direction are considered. The measured response is used for filter, amplifier, and coaxial cable. The variation of amplifier gain up to 15% in amplitude due to temperature dependence is taken into account. The noise is generated by adding forced-trigger event to the simulated signal.

The detection efficiency of individual showers is evaluated with a trigger simulation where showers are divided into energy, zenith and azimuth bins for calculating the average detection efficiency of a specific bin, $\varepsilon_{det}(E,\theta,\phi)$. The areal acceptance (in unit of km^2 sr) can be obtained by multiplying the efficiency by the full simulated area and the solid angle per bin, summed over all angular bins, $\langle A(E)\rangle_\Omega = \sum_{\theta,\phi}\varepsilon_{det}(E,\theta,\phi)A_{MC}\Delta\Omega$. The expected number of events is calculated by $N = T_{live}\int\langle A(E)\rangle_\Omega F(E)dE$, where T_{live} stands for station live time, $F(E)$ for cosmic-ray flux (in unit of km^{-2} s^{-1} sr^{-1} eV^{-1}). Fig. 2 shows the expected areal acceptance and resulting event distribution using the cosmic ray flux observed by Pierre Auger Observatory [15] (with extrapolation at lower energy end) and a live time of 81.8 days for 2017-2018 data. The detection threshold of HCR station is around 300 PeV, and most of cosmic-ray events come from zenith angle $\theta = 65°$–$85°$, with total number of 180 events.

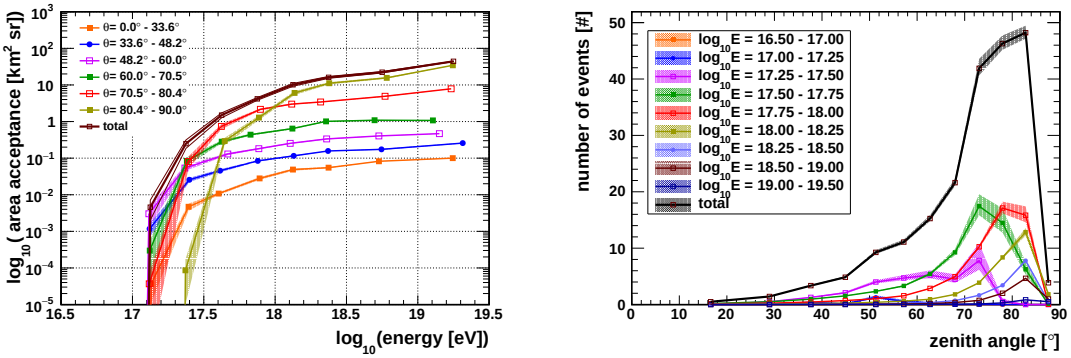

Figure 2: Left: expected cosmic-ray area acceptance of HCR station versus energy for different zenith angles. Right: expected angular distribution of cosmic ray events, assuming Auger CR spectrum and exposure of 81.8 days. The shaded area shows the uncertainty due to 15% variation of amplifier gain.

It is notable that including the reflection interference leads to an increase in total event rate by about 40%, mostly contributed by events of lower energy of 0.3–1 EeV and larger zenith angle of 65° to 85°. This is because the station have antennas at different heights and hence reflection delays, which are of order of several ns at these angles, likely causing both constructive and destructive interference among them. The 3 out of 8 coincidence trigger would then pick up those constructive ones, and make these weaker, less energetic events (of higher flux) around the trigger threshold more detectable.

Cosmic-ray events of zenith above 85° are suppressed due to both farther distance to the shower and destructive interference with the reflected signal (as reflection delays become subnanosecond and the polarization is inverted when reflecting off the snow surface). The former factor can make showers induced by mountain-skimming tau neutrinos at closer distance more distinguishable, while for the latter it requires a more realistic model of snow surface considering the roughness and diffuse scattering.

5. Cosmic ray search and background rejection

A preliminary search for cosmic-ray signals is performed on the available dataset of the 2017–18 season. The data starting from 2017-11-26 to 2018-04-10 with a live time of roughly 81.8 days,

consists of 199,476 normal-trigger events plus 105,494 forced-trigger events.

The RF background has the same characteristics as reported in the prototype [7]. The spectrum of noise background is dominated by Galactic noise below 300 MHz, and by thermal noise above. The majority of the events comes from two noise categories: one associated with satellite or air traffic communication shows power excess above the background at 240–280 MHz and 350–390 MHz band. The other type are correlated with periods of high wind speed (> 15 m/s), usually appeared in groups within hours or days together with high event rate. These events are characterized by anomalously large amplitudes and spectral power in the low stopband at only few channels of the same tower. In contract to these noise, cosmic-ray signals are relatively rare, Hpol-dominated, and broadband with higher power at lower frequencies.

Given the above properties, an event selection is performed with a spectral analysis. The parameters are defined and cuts are set based on distribution of forced-trigger events, as following:

- high Hpol to Vpol power ratio at lower passband of 110–230 MHz, $P[110,230]$. The threshold is set at around 4 dB, at 5σ right of distribution of forced-trigger events;
- high power ratio $P[110,230]/(P[240,280]+P[350,380]) > 0$ dB for all Hpols, to reject satellite communication noise;
- high ratio $P[110,230]/P[60,110] > 1$ dB for all Hpols, to reject high-wind events;
- low ratio of max to min power $P[110,230]$ between Hpols on different towers, < 5 dB for channel similarity, to reject high-wind events.

1,478 events are selected after the cuts, which preserves about 92% of CR events according to the simulation. These events are then reconstructed with plane wave assumption. A reconstruction quality cut requires the average cross-correlation coefficient (between $[0,1]$) > 0.7. Events with reconstructed zenith $> 85^\circ$ are excluded from the analysis, since the direct and reflected signals are largely overlapped at these angles and can cause error of several degrees and misidentification as neutrino signal, and the algorithm for disentangling has not been fully developed yet. Lastly, a time cluster cut requires that a candidate should have no adjacent events within ± 1000 seconds.

After all selections are applied, 85 cosmic-ray candidates are identified. A candidate is shown in Fig. 3 and the temporal distribution of events in Fig. 4. To reduce the interference from reflection to obtain a more accurate direction, the reconstruction is re-processed with waveforms deconvolved with the antenna response at previously reconstructed angles, assuming they are close to real angles and the antenna response varies slowly around its main lobe. The deconvolved waveforms in Fig. 3 show that the zenith angle can be also inferred from the TDOA of reflected signals between top and bottom channels, if any one of them is resolvable from the direct one.

The observed and expected zenith distributions of candidates events are shown at the right of Fig. 4. The estimated analysis efficiency of each cut is listed in Table 1 The observation has comparable number of events with the simulation with all analysis cuts applied (85 vs 95.8). However, the analysis efficiency is only about 50% and there is discrepancy in the angular distribution around $\theta = 70^\circ - 80^\circ$, indicating the events here were mis-reconstructed and got rejected. A more robust reconstruction method is in progress to solve the problem.

6. Ongoing and Future Works

As the source direction is essential for distinguishing between cosmic-ray and neutrino sig-

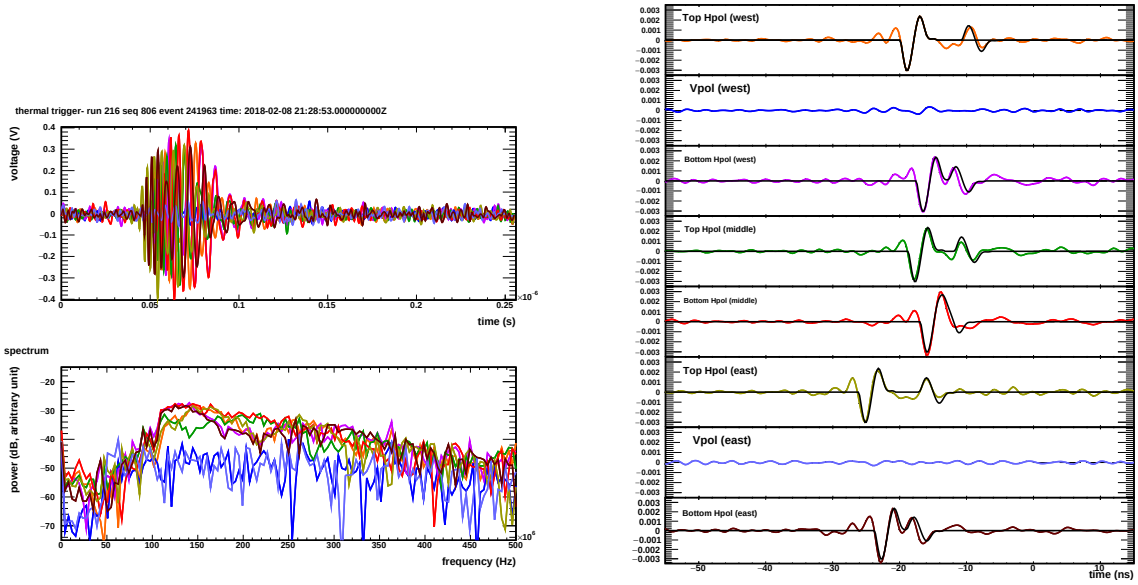

Figure 3: Left: waveforms (top panel) and power spectra (bottom) of a cosmic-ray candidate with reconstructed (azimuth, zenith) angle = $(-12.5°, 71.0°)$. Right: waveforms after deconvolving receiver response (in the order of west to east tower, upper to lower antenna), in which clear reflected pulses can be seen. The leading bipolar pulse shown in black at the top panel (top Hpol at west tower) is used as template to model the expected direct and reflected pulses of all Hpol channels.

	triggered	spectral	correlation > 0.7	zenith angle $> 85°$	all cuts
number of events	180.6	167.8	127.9	127.0	95.8
efficiency	100%	92.9%	70.8%	70.3%	53.0%

Table 1: Expected number of events and analysis efficiency for each selection cut applied in the preliminary analysis, estimated by the simulation.

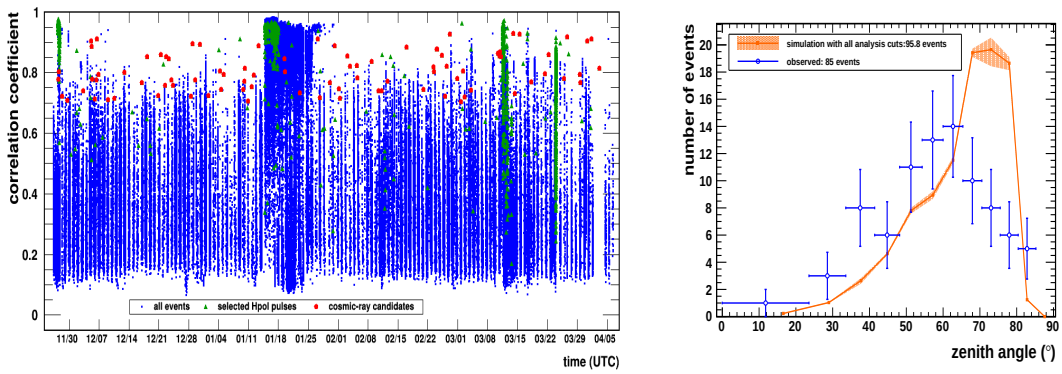

Figure 4: Left: average cross-correlation coefficient of event reconstruction of 2017-18 data, where blue dots for all events, green triangles for those passing spectral cuts, and red circles for 85 CR candidates. The quasi-periodic vertical stripes of events are daily variation of the Galactic noise level and sat. comm. noise, and the cluster of high-correlation events during Jan. 16–26 are from Mt. Discovery pulser. Right: zenith angle distribution of 85 cosmic-ray candidates, compared with the simulated one with all selection cuts applied (95.8 events expected). True angle rather than the reconstructed one is used for simulated curves.

nals, a more effective way for unfolding the reflection and receiver response at inclined angles is needed to improve event reconstruction and the analysis efficiency. One method is the forward folding technique [16] applied to in-ice ARIANNA stations for reconstructing the electric field and estimating energy of cosmic ray [4]. On the other hand, as the cosmic-ray event rate is sensitive to the threshold due to its spectrum, more realistic modelling of antenna response with interference from the firn and nearby structures, snow surface with roughness, and *in-situ* trigger calibration need to be take into account for more accurate simulation and analysis.

7. Acknowledgements

We wish to thank the US National Science Foundation for its support of the ARIANNA project under grant PHY-1607719, support from National Research Nuclear University MEPhI (Moscow Engineering Physics Institute), from the German Research Foundation (DFG), and for the outstanding cooperation in field planning and operations by the Antarctic Support Contractor. The project is also supported by the pioneer program of Ministry of Science and Technology (MOST) in Taiwan.

References

[1] F. Schröder, *Prog. Part. Nucl. Phys.* **93** (2017) 1 [astro-ph/1607.08781].

[2] H. Schoorlemmer et al., *Astropar. Phys.* **77** (2016) 32 [astro-ph/1612.04473].

[3] S. Barwick et al., *Astropar. Phys.* **90** (2017) 50 [astro-ph/1506.05396].

[4] A. Nelles et al. (the ARIANNA Collaboration), PoS(ICRC2019)366.

[5] P. Gorham et al., *Phys. Rev. Lett.* **121** (2018) 161102.

[6] J. Nam and T. Liu, PoS(ICRC2017)944.

[7] S. Wang et al. (the TAROGE and the ARIANNA Collaborations), PoS(ICRC2017)358

[8] C. Persichilli et al. (the ARIANNA Collaboration), PoS(ICRC2019)980

[9] A. Anker et al., *Advances in Space Research* (2019) [astro-ph/1903.01609]

[10] S. Kleinfelder, E. Chiem, and T. Prakash, *Proc. of 2014 IEEE NSS/MIC* (2014) 1 [physics/1505.07085]

[11] A. Romero-Wolf et al., *Astropar. Phys.* **60** (2015) 72 [astro-ph/1304.5663]

[12] P. Gorham et al., *Phys. Rev. D* **98** (2018) 042004.

[13] T. Huege, M. Ludwig, and C. James, AIP Conference Proceedings **1535** (2013) 128.

[14] High-Frequency Structure Simulator (HFSS) 15.0.3 software, Ansoft Corporation.

[15] F. Fenu et al. (the Pierre Auger Collaboration), PoS(ICRC2017)486

[16] C. Glaser et al., *Eur. Phys. J. C*, **79** (2019) 464 [astro-ph/1903.07023]